Kinematics Model of Bionic Manipulator by Using Elliptic Integral Approach

Mrunal K. Mishra, Arun K. Samantaray, Goutam Chakraborty, Vipin Pachouri, Pushparaj Mani Pathak, and Rochdi Merzouki

Abstract This paper suggests a variable curvature kinematics model for the bionic continuum robots (BCRs) using elliptic integral approach. For the BCR, the manipulator is assumed to be a flexible beam, in which a large deflection takes place due to external loadings. A six-DoF elephant trunk-like BCR known as Robotino-XT is considered here for study. The external load is assumed to be an equivalent moment calculated from the pneumatic forces applied on the bellow tube-like actuators. Optitrack motion-sensing vision system with Motive 2.0 interface is used to acquire the deflection and orientation of the tip of the trunk. The analytical results are validated with experimental data.

Keywords Bionic manipulator · Elliptic integral · Large deflection · Variable curvature modelling

1 Introduction

Soft continuum robotics deals with flexible robots with high degrees of freedoms (DoFs). This particular class of robots is inspired by biological creatures such as snakes [1], elephant trunks [2] and so forth. These robots accomplish their movement by the principle of high deformation (also called compliant mechanism) of their members. No assembly, less wear and more workspace are some of the significant advantages of the compliant mechanisms over rigid systems. Under the same force,

M. K. Mishra (✉) · A. K. Samantaray · G. Chakraborty
Indian Institute of Technology Kharagpur, Kharagpur 721302, India
e-mail: mrunalkanti@gmail.com

A. K. Samantaray
e-mail: samantaray@mech.iitkgp.ac.in

V. Pachouri · P. M. Pathak
Indian Institute of Technology Roorkee, Roorkee 247667, India

R. Merzouki
Université de Lille, 59655 Lille, France

R. Kumar et al. (eds.), *Machines, Mechanism and Robotics*, Lecture Notes in Mechanical Engineering, https://doi.org/10.1007/978-981-16-0550-5_30

compliant mechanisms provide more significant deflection than their rigid counterparts, thus making the bionic manipulators more dexterous. However, the high dexterity of these manipulators is achieved at the cost of more material and system nonlinearities.

To date, forward kinematics developed for BCRs are mostly based on piecewise constant curvature assumption [3]. This procedure describes the state of the distorted backbone of the BCRs with a constant curvature curve. However, models developed with this approach do not correlate well with the biological counterparts because of the assumed constant circular section of the backbone curve. On the contrary, a variable curvature approach for multi-sectional BCRs has been proposed to achieve the exact shape of the backbone [4]. The curvature models work with two sub-mappings, i.e. explicit mapping and typical mapping. There are several other benchmark models developed to determine the forward kinematics (FK) of a BCR. Cosserat continuum theory model [5] and modal method [6] are the other methods used to establish forward kinematics of hyper-redundant manipulators. Although these models are accurate, they are not suitable for real-time control applications because of their high computational complexity.

BCRs accomplish their movement by the principle of high deformation of their members. So, these robots can be assumed as cantilever beams with large deflection under loading. Large deflection of cantilever beams is solved by minimising the integral of the residual error of the governing differential equation of the beam [7]. The very same problem can also be solved by using the elliptic integral approach [8, 9].

In this paper, a novel method is proposed for the FK of the BCRs in Sect. 2. Section 3 describes the experimental set-up for Robotino-XT. The implementation and validation of the analytical results with experimental observations are given in Sect. 4. Finally, the concluding remarks are presented in Sect. 5.

2 System Configuration

The trunk of Robotino-XT consists of two segments, where each segment includes three individual pressure-actuated bellow tubes, as shown in Fig. 1a. The bellow tubes are equidistant from the centre of the manipulator with actuator spacing of 120°. The 4.12° tapered conical-shaped bellow tubes are made of polyamide material with a laser sintering process. The resultant differential pressure force in bellows creates a bending moment, which bends the segment about x-y axes, but there is no twist about the z-axis. Also, an inextensible wire passing through the centre of the assembly constrains the mean length, i.e. the neutral axis of the equivalent beam has a constant length.

The resultant bending moment at the head of the section is found by taking a moment of all the forces in Fig. 1b about the centre and obtained as

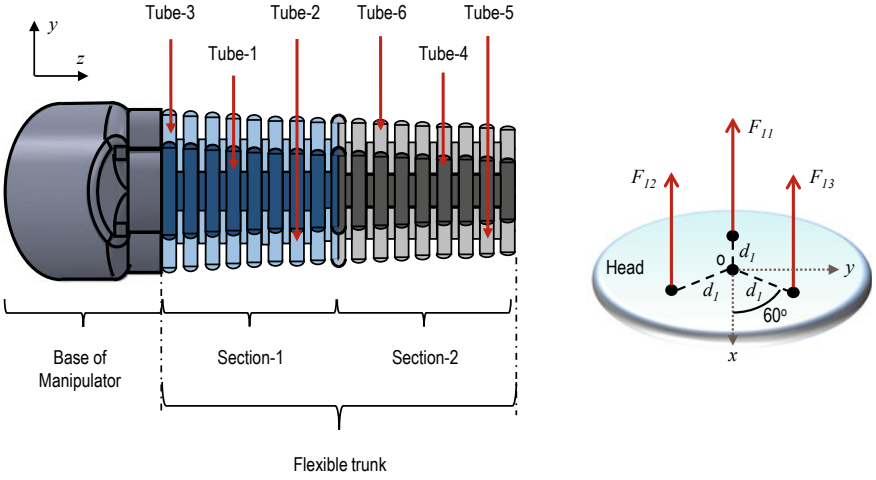

Fig. 1 **a** Robotino-XT projected view, **b** forces at the head of the first segment

$$M_e = (F_{i3} - F_{i2})\frac{\sqrt{3}d_1}{2}\hat{i} + \left(F_{i1} - \frac{F_{i2} + F_{i3}}{2}\right)d_1\hat{j} \tag{1}$$

where the first subscript to forces (F) or pressure (P) denotes the segment number and the second denotes the tube number.

The current study is focused only on the first section of the trunk. Moreover, it is assumed that the trunk of the Robotino-XT is rotated only about the y-axis. As such, the study is strictly directed towards planar motions of the first trunk segment within the z-x plane. It is also to be noted that such planar motion is conceivable only if the same actuation pressures are applied in tube-2 and tube-3 simultaneously, as shown in Fig. 1b. Furthermore, for the sake of convenience, the trunk weight is also neglected in mathematical modelling.

The trunk of the Robotino-XT is considered to be a flexible cantilever beam (neutral axis is assumed to inextensible) having a variable cross section, length L and modulus of elasticity E. The beam is subjected to an equivalent bending moment M_e and a point load W inclined an angle β from the z-axis as shown in Fig. 2. A new variable s is introduced for the curvilinear coordinate along the deflected axis of the beam. The exclusion of self-weight leads the external end-effector load W to be independent of arc length s. By applying the usual Euler–Bernoulli beam theory assumptions, the equilibrium equation for the moment can be written as

$$\mathrm{EI}(s)\frac{\mathrm{d}\theta(s)}{\mathrm{d}s} = M_{(z,x)} = W_x(z_0 - z) + W_z(x_0 - x) + M_e \tag{2}$$

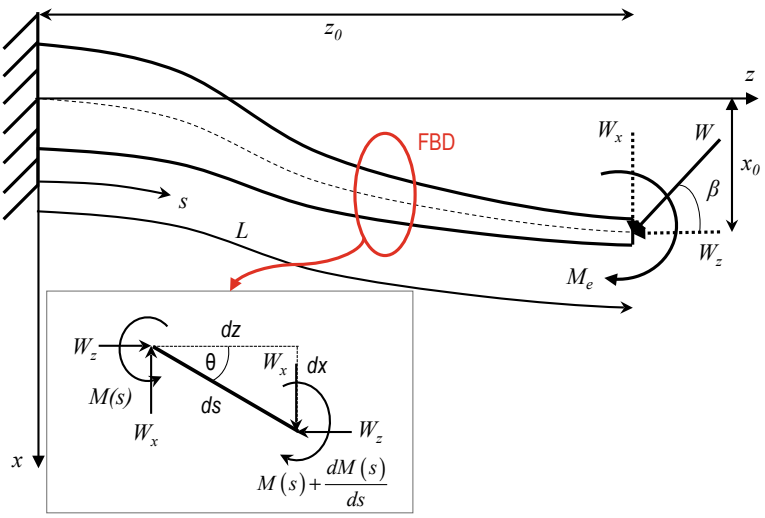

Fig. 2 An equivalent cantilever beam

where (z_0, x_0) is the location of the tip of the deflected beam, W_z, W_x are the respective z and x components of the load W, $EI(s)$ is the variable flexural rigidity and $\theta(s)$ is the slope of the beam.

Differentiating (2), the force balance equation can be written as

$$EI(s)\frac{\mathrm{d}^2\theta(s)}{\mathrm{d}s^2} = -W_z\sin(\theta(s)) - W_x\cos(\theta(s)) \tag{3}$$

where $\frac{\mathrm{d}x}{\mathrm{d}s} = \sin(\theta(s))$, $\frac{\mathrm{d}z}{\mathrm{d}s} = \cos(\theta(s))$ (from FBD of Fig. 1a).

This cantilever beam is associated with two boundary conditions: $\theta(s)$ at fixed end is 0 and slope $\frac{\mathrm{d}\theta(s)}{\mathrm{d}s}$ at free end is $\frac{M_e}{\mathrm{EI}(L)}$.

The equivalent moment is $(M_e) = \pi\left(r_1 - L_1\tan\left(\frac{\phi}{2}\right)\right)^2 P_{11}d_1$ and the variable moment of inertia is $I(s) = I_0\left(\alpha_{11}(1-k_{11}s)^4 - \alpha_{12}(1-k_{12}s)^4\right)$ where I_0 is the moment of inertia at the fixed end and $\alpha_{11} = \frac{R_1^4}{R_1^4 - r_1^4}$, $\alpha_{12} = \frac{r_1^4}{R_1^4 - r_1^4}$, $k_{11} = \frac{\tan\phi}{R_1}$, and $k_{12} = \frac{\tan\phi}{r_1}$. So, (3) can be written in elliptic integral form as

$$\int \frac{\mathrm{d}s}{\sqrt{I(s)}} = \varsigma\sqrt{\frac{E}{W}}\int \frac{\mathrm{d}x_1}{\sqrt{\left(1-x_1^2\right)\left(1-\varsigma^2x_1^2\right)}}. \tag{4}$$

Integrating (4) and applying the boundary conditions, one obtains [9]

$$x_1 = sn\left[\frac{Ws}{\mathrm{EI}\varsigma} + F(\sin(\beta/2);\varsigma);\varsigma\right] \tag{5}$$

where $sn[u; m]$ is a Jacobian elliptic function (refer [8] for more details). The slope of the beam in terms of non-dimensional parameters can be written as

$$\theta(\overline{s}) = 2\sin^{-1}\left(sn\left[\frac{\overline{\omega s}}{\varsigma} + F(\sin(\beta/2); \varsigma); \varsigma\right]\right) - \beta \tag{6}$$

where $\overline{s} = \frac{s}{L}$, $\overline{\omega}^2 = \frac{WL^2}{\mathrm{EI}}$ are non-dimensional parameters. Inserting (6) into $\frac{\mathrm{d}x}{\mathrm{d}s} = \sin(\theta(s))$, $\frac{\mathrm{d}z}{\mathrm{d}s} = \cos(\theta(s))$, and integrating, the tip position can be found.

3 Experimental Set-Up

Figure 3a depicts the experimental set-up which comprises a flexible continuum trunk (manipulator) and an external observer (Optitrack motion sensor). In this experiment, the motion tracking system utilises Motive 2.0 software, four Prime 13 cameras and nine retro-reflective markers to capture the motion of an object. Prime 13 cameras are equipped with an optical lens of 8 mm F 1.8 and a stock lens of 5.5 mm F 1.8, which has high-resolution image sensing (1280 × 1024) capacity. These cameras track any surfaces covered with retro-reflective material, as shown in Fig. 3b. This material is intended to reflect the approaching light to its source origin. Infrared light radiated from the camera is reflected by the markers and identified by the camera's sensor. The captured reflections are utilised to ascertain the 2D marker positions, which are utilised by Motive 2.0 to estimate the corresponding 3D positions through reconstruction. In the Motive 2.0 interface, three markers at each section are selected together as a rigid body (as shown by the red dashed triangle in Fig. 3b).

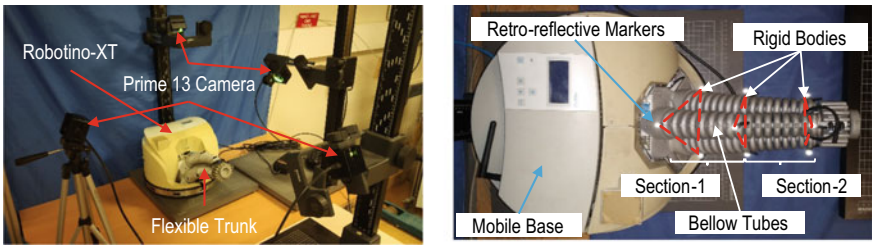

(a) (b)

Fig. 3 **a** Robotino-XT test bench with vision system, **b** Robotino-XT with retro-reflective markers

4 Results and Discussion

A series of gauge pressures are applied to tube-1 (while keeping 0 (atmospheric) pressures in other tubes), or equal pressures in tubes 2 and 3 (while keeping tube-1 pressure 0), to see the effect of tip deflection and orientation with respect to the mean position in the x-z plane. The gauge pressure is varied from 0 to 1.7 bar with an increment of 0.05 bar through a compressor and two-way solenoid valve arrangement, which is controlled by an internal PID controller. The dashed blue line, as shown in Fig. 4a, is the tip position of section-1 of the trunk. For the analytical study, an equivalent moment is applied on the tip of the tapered beam. The parameters used for the large deflection of the beam are as modulus of elasticity $E = 6.16 \times 10^6$ N/m^2, length of the beam $L_1 = 10.14$ cm, outer bellow base radius $R_1 = 2.685$ cm and inner bellow base radius $r_1 = 2.535$ cm, with an equivalent wall thickness of 1.5 mm. In the present study, the reference tip frame is taken at the position of static deflection of the trunk. Figure 4a shows the tip position of the beam and the first section head position of the trunk. The tip of the proposed equivalent tapered beam starts from (101.40, 0 mm) with 0 bar pressure and ends at (84.044, 56.1957 mm) with 1.7 bar pressure. On the other hand, the tip of the trunk starts from (101.40, 0 mm) with 0 bar pressure and ends at (87.51, 55.53 mm) with 1.7 bar pressure. It can also be seen that up to 1.05 bar, both experimental and analytical results match perfectly and then the results slightly diverge. This is possibly due to existing material non-linearity or elastic extension of the wire used to constrain the backbone length. The black dotted lines in Fig. 4a show the shape of the elastic curve of the beam. Overall, a good match is found between the numerical and experimental results. As for the tip orientation in the x-z plane (θ_y), it can be seen from Fig. 4b that the numerical and experimental results nearly match for the allowable range of pressure in the bellow tubes. The maximum tip angle from the z-axis for the experimental study is 35.603°, and that from the numerical study is 36.38°. An appropriately designed closed-loop position controller can compensate for these small modelling errors.

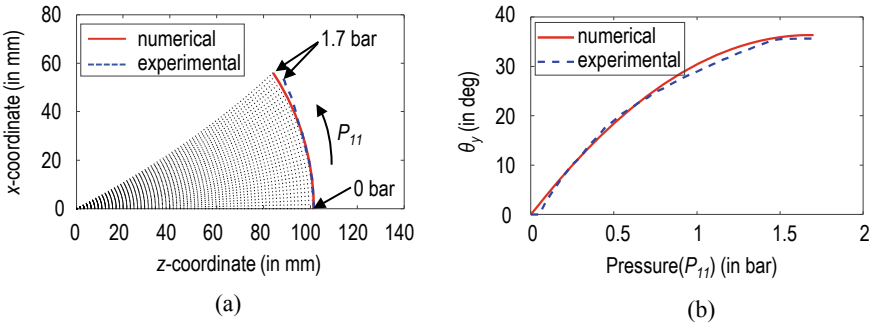

Fig. 4 **a** Tip deflection, **b** tip orientation

5 Conclusions

A general closed-form solution for orientation and deflection of the cantilever beam is obtained by using the elliptic integral approach, which satisfies the boundary conditions. Experimental results are obtained from Robotino-XT by using the Optitrack motion sensor. Finally, the developed analytical method is validated with the experimental results obtained from the flexible continuum trunk Robotino-XT. A good match is found between the numerical and experimental results for both tip deflection and orientation of the trunk. Further study including the weight of the trunk as well as the spatial movement of the trunk, i.e. inertial forces, will be taken up as future research work.

Acknowledgements This work was supported by the joint collaborative research project between DST (India), Indo French Centre for the Promotion of Advanced Research (IFCPAR) and CNRS in France (PRC CNRS-DST 2016-2018).

References

1. Khan R, Watanabe M, Shafie AA (2010) Kinematics model of snake robot considering snake scale. Am J Appl Sci 7(5):669–674
2. Robotino XT. https://www.festo.com/group/en/cms/10239.htm
3. Mishra MK, Samantaray AK, Chakraborty G, Jain A, Pathak PM, Merzouki R (2019) Dynamic modelling of an elephant trunk like flexible bionic manipulator. In: Proceedings of the 2019 IMECE, 4. ASME, Salt Lake City, pp 1–9
4. Mahl T, Hildebrandt A, Sawodny O (2014) A variable curvature continuum kinematics for kinematic control of the bionic handling assistant. IEEE Trans Rob 30(4):935–949
5. Chirikjian GS (2015) Conformational modeling of continuum structures in robotics and structural biology: a review. Adv Robot 29(13):817–829
6. Chirikjian GS, Burdick JW (1994) A modal approach to hyper-redundant manipulator kinematics. IEEE Trans Robot Autom 10(3):343–354
7. Dado M, Al-Sadder S (2005) A new technique for large deflection analysis of non-prismatic cantilever beams. Mech Res Commun 32(2005):692–703
8. Abu-Alshaikh I, Alkhaldi HS, Beithou N (2018) Large deflection of prismatic cantilever beam exposed to combination of end inclined force and tip moment. Mod Appl Sci 12(1):98–110
9. Kimball C, Tsai LW (2002) Modelling of flexural beams subjected to arbitrary end loads. J Mech Des 124:223–235